**Supporting Information**

# Different Effects of a Co-template and $[TM(phen)_m]^{2+}$ ($m$ = 1–3) Complex Cations on the Self-assembly of a Series of Hybrid Selenidostannates Showing Combined Optical Properties of Organic and Inorganic Components

Guang-Ning Liu, Guo-Cong Guo,* Ming-Jian Zhang, Jin-Shuang Guo, Hui-Yi Zeng, and Jin-Shun Huang

*State Key Laboratory of Structural Chemistry, Fujian Institute of Research on the Structure of Matter, Chinese Academy of Sciences, Fuzhou, Fujian 350002, P. R. China*

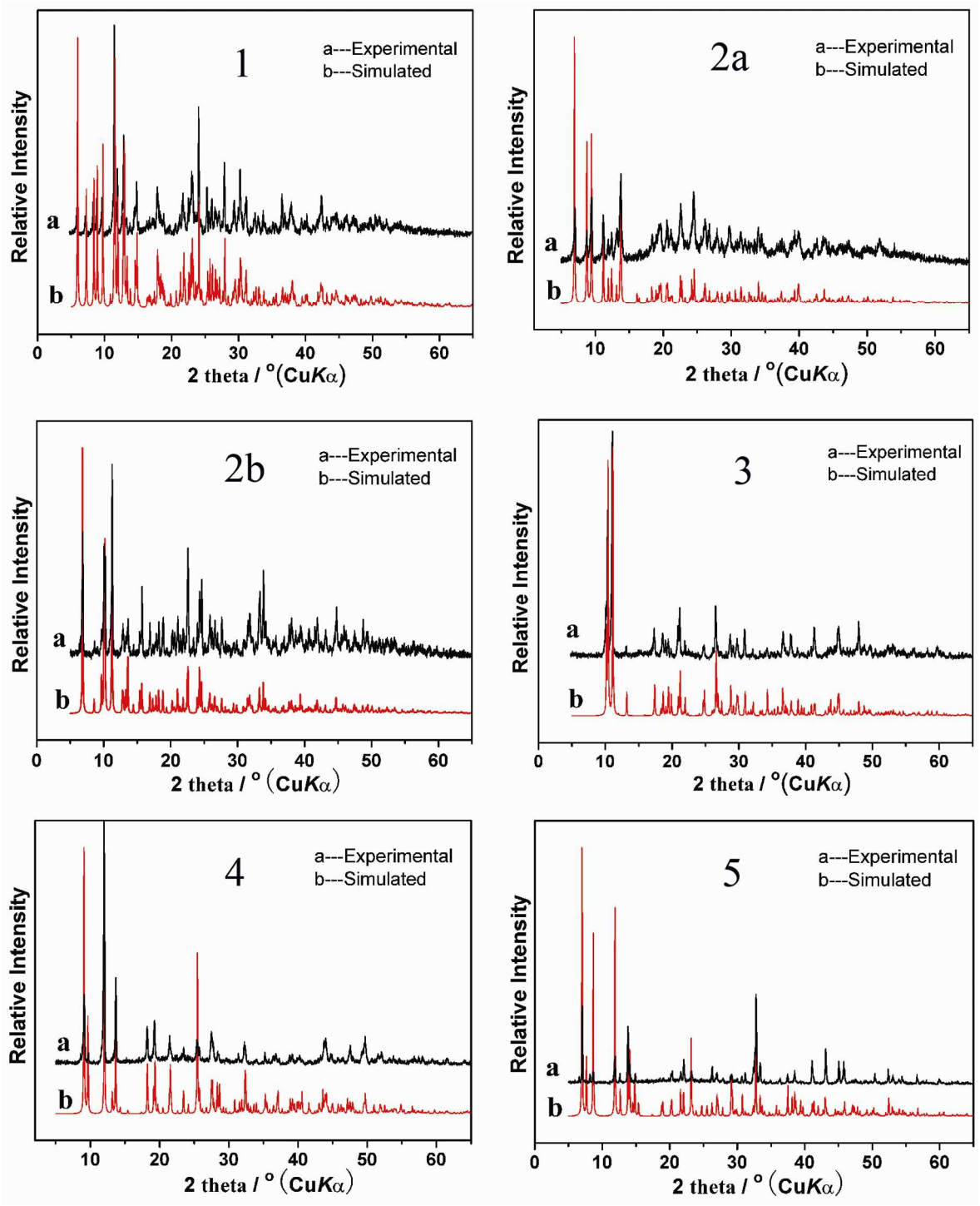


**Figure S1.** The experimental PXRD patterns of **1–5** (black) are in good agreement with their corresponding simulated PXRD patterns calculated from single-crystal X-ray data (red).

**Table S1.** Ranges of Selected Bond Distances (Å) and Angles (°) for **1–5**.

| **1** | | | |
|---|---|---|---|
| Sn–Se | 2.452(1)–2.602(1) | Se–Sn–Se | 93.654(13)–114.833(18) |

| | | | |
|---|---|---|---|
| Sn–Se–Sn | 86.346(13) | | |
| | | **2a** | |
| Sn–Se | 2.477(1)–2.582(1) | Mn–Se | 2.672(1)–2.704(1) |
| Mn–N | 2.292(2)–2.373(2) | Se–Sn–Se | 93.96(2)–117.36(2) |
| Sn–Se–Sn | 86.04(2) | N–Mn–N | 70.97(8)–149.77(8) |
| N–Mn–Se | 89.69(5)–170.56(6) | Se–Mn–Se | 92.48(2) |
| | | **2b** | |
| Sn–Se | 2.468(1)–2.576(1) | Fe–Se | 2.599(1)–2.615(1) |
| Fe–N | 2.187(2)–2.263(2) | Se–Sn–Se | 95.01(1)–117.61(1) |
| Sn–Se–Sn | 84.993(11) | N–Fe–N | 73.96(8)–153.07(8) |
| N–Fe–Se | 87.95(5)–172.86(6) | Se–Fe–Se | 93.97(1) |
| | | **3** | |
| Sn–Se | 2.468(2)–2.559(1) | Mn–Se | 2.608(1)–2.742(2) |
| Mn–N | 2.236(3)–2.247(3) | Se–Sn–Se | 95.52(4)–118.46(3) |
| Sn–Se–Sn | 84.48(4) | N–Mn–N | 74.22(10) |
| N–Mn–Se | 91.36(8)–162.86(6) | Se–Mn–Se | 92.85(5)–102.34(3) |
| | | **4** | |
| Sn–Se | 2.454(1)–2.574(1) | Mn–Se | 2.682(1) |
| Mn–N | 2.278(3)–2.375(3) | Se–Sn–Se | 93.83(2)–118.81(2) |
| Sn–Se–Sn | 86.17(2)–97.93(3) | N–Mn–N | 71.69(8)–145.37(13) |
| N–Mn–Se | 91.37(5)–161.02(5) | Se–Mn–Se | 104.45(3) |
| | | **5** | |
| Sn–Se | 2.515(1)–2.798(1) | Fe–N | 1.970(3)–1.977(3) |
| Se–Sn–Se | 86.98(1)–176.09(2) | Sn–Se–Sn | 85.64(1)–96.02(2) |
| N–Fe–N | 83.13(11)–173.22(10) | | |

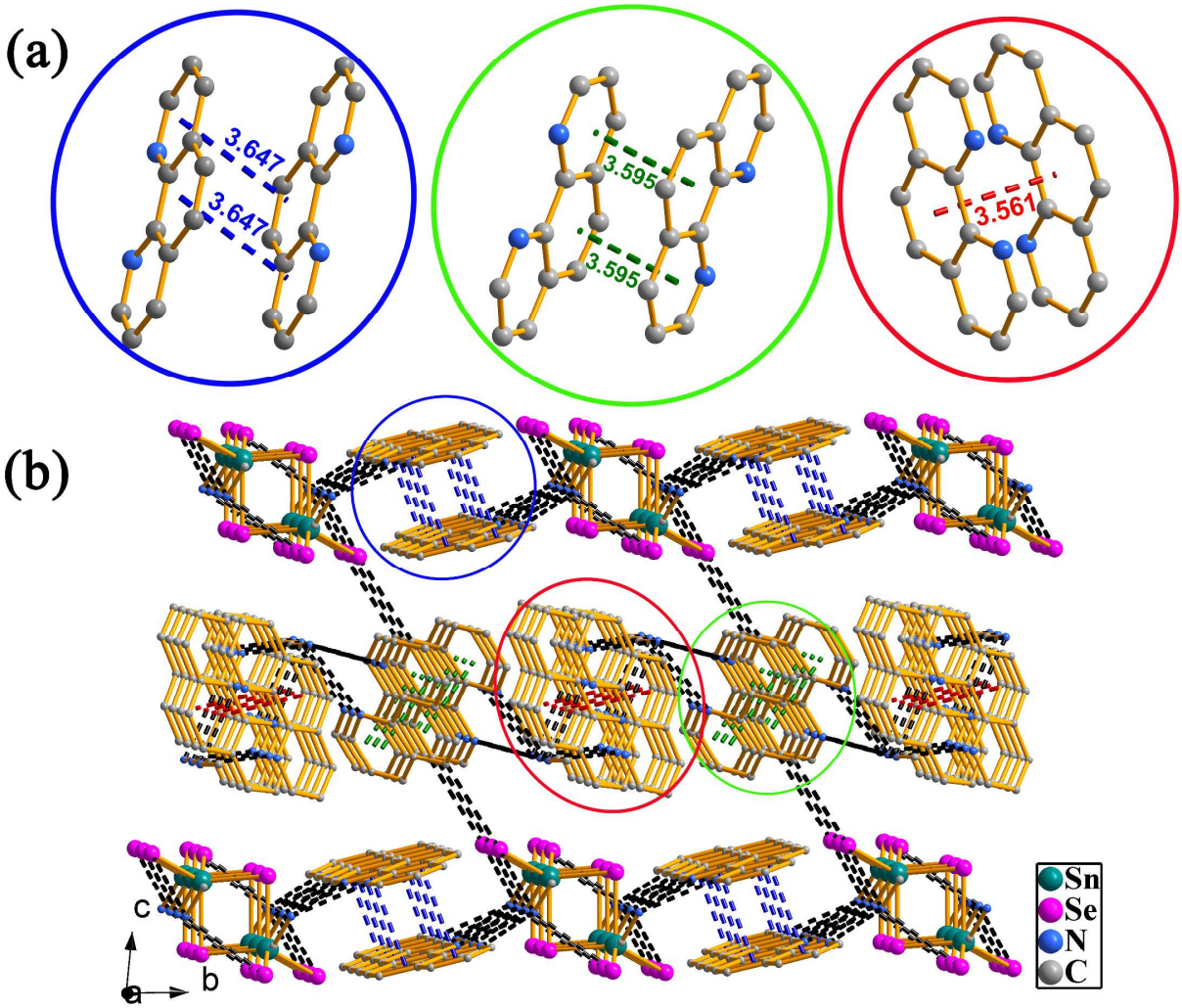


**Figure S2.** (a) View of three kinds of face-to-face $\pi\cdots\pi$ stacking interactions in **1** (shown in blue, green, and red dashed lines, respectively). (b) View of a 3-D supramolecular network of **1** along the *a* axis showing C–H···Se, N–H···Se and N–H···N hydrogen bonds (black dashed lines) and face-to-face $\pi\cdots\pi$ stacking interactions. Hydrogen atoms are omitted for clarity.

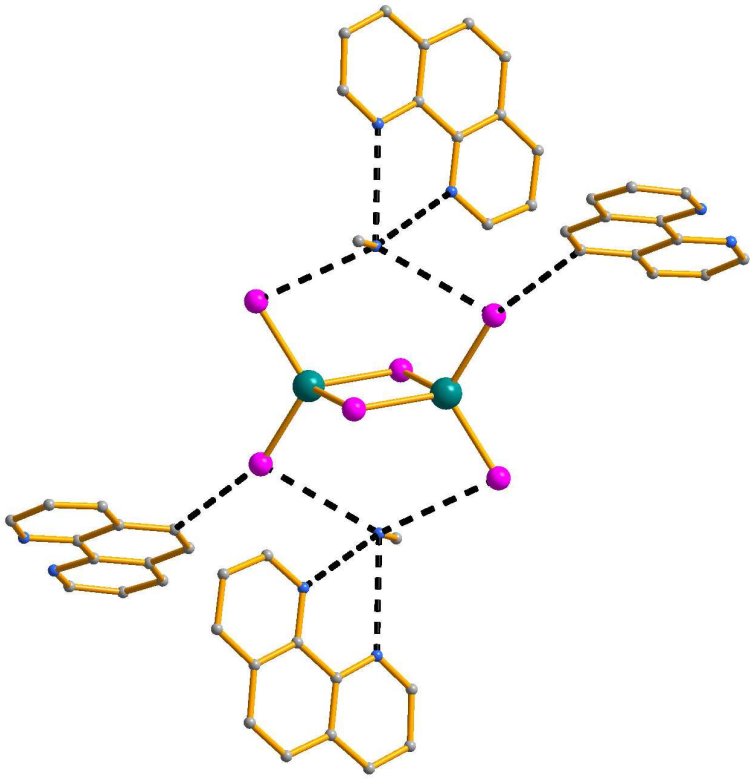

**Figure S3.** View of surrounding of a $(Sn_2Se_6)^{4-}$ anion in **1**, showing the hydrogen bonds between the co-template and the $(Sn_2Se_6)^{4-}$ anion (black dashed lines).

**Table S2.** Selected Hydrogen Bonds Data for **1**.

| D–H···A | D–H (Å) | H···A (Å) | D···A (Å) | ∠(DHA) (°) |
|---|---|---|---|---|
| N1–H1C···Se3 | 0.89 | 2.61 | 3.471(3) | 164 |
| N1–H1A···Se1[a] | 0.89 | 2.61 | 3.451(3) | 159 |
| N1–H1B···N11[b] | 0.89 | 2.23 | 3.083(3) | 160 |
| N1–H1B···N12[b] | 0.89 | 2.36 | 2.978(4) | 127 |
| N2–H2B···N21 | 0.89 | 2.12 | 2.937(5) | 152 |
| N2–H2B···N22 | 0.89 | 2.61 | 3.270(5) | 132 |
| N2–H2C···N31 | 0.89 | 2.17 | 2.883(5) | 137 |
| N2–H2C···N32 | 0.89 | 2.36 | 3.156(5) | 148 |
| C36–H36A···Se1[c] | 0.93 | 2.93 | 3.826(4) | 163 |

Symmetry codes: a 2-x, 1-y, 2-z; b x, -1+y, z; c 2-x, 2-y, 1-z.

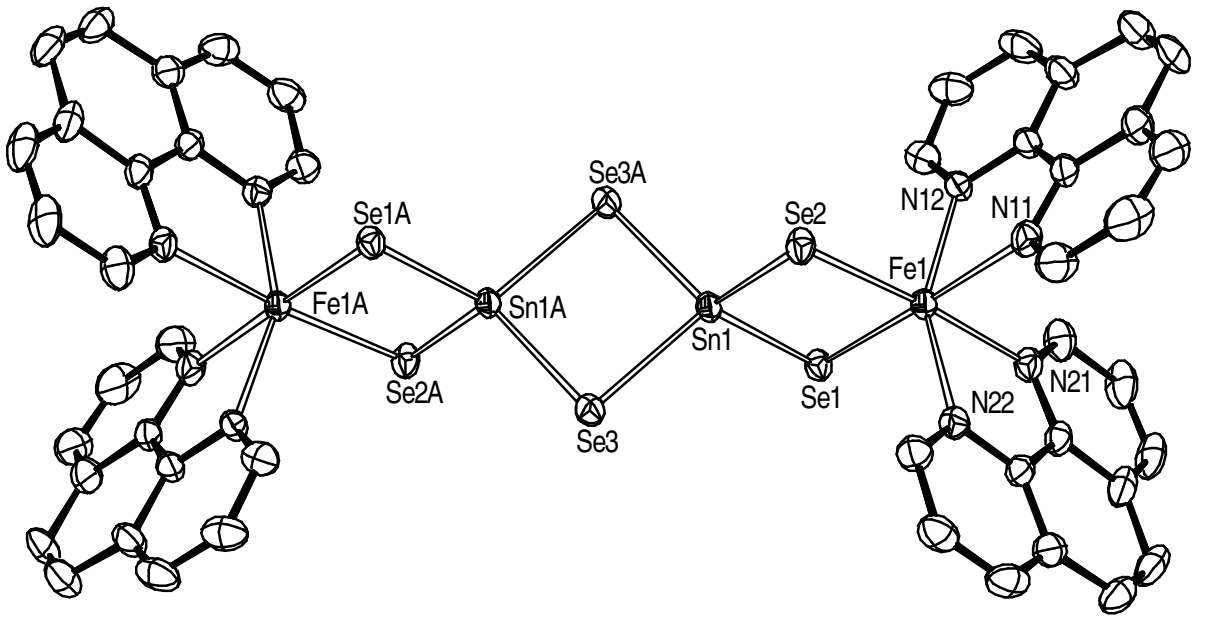


**Figure S4.** ORTEP drawing of **2b** with 30% thermal ellipsoids and hydrogen atoms being omitted for clarity. Symmetry code: A (1-x, 2-y, 1-z).

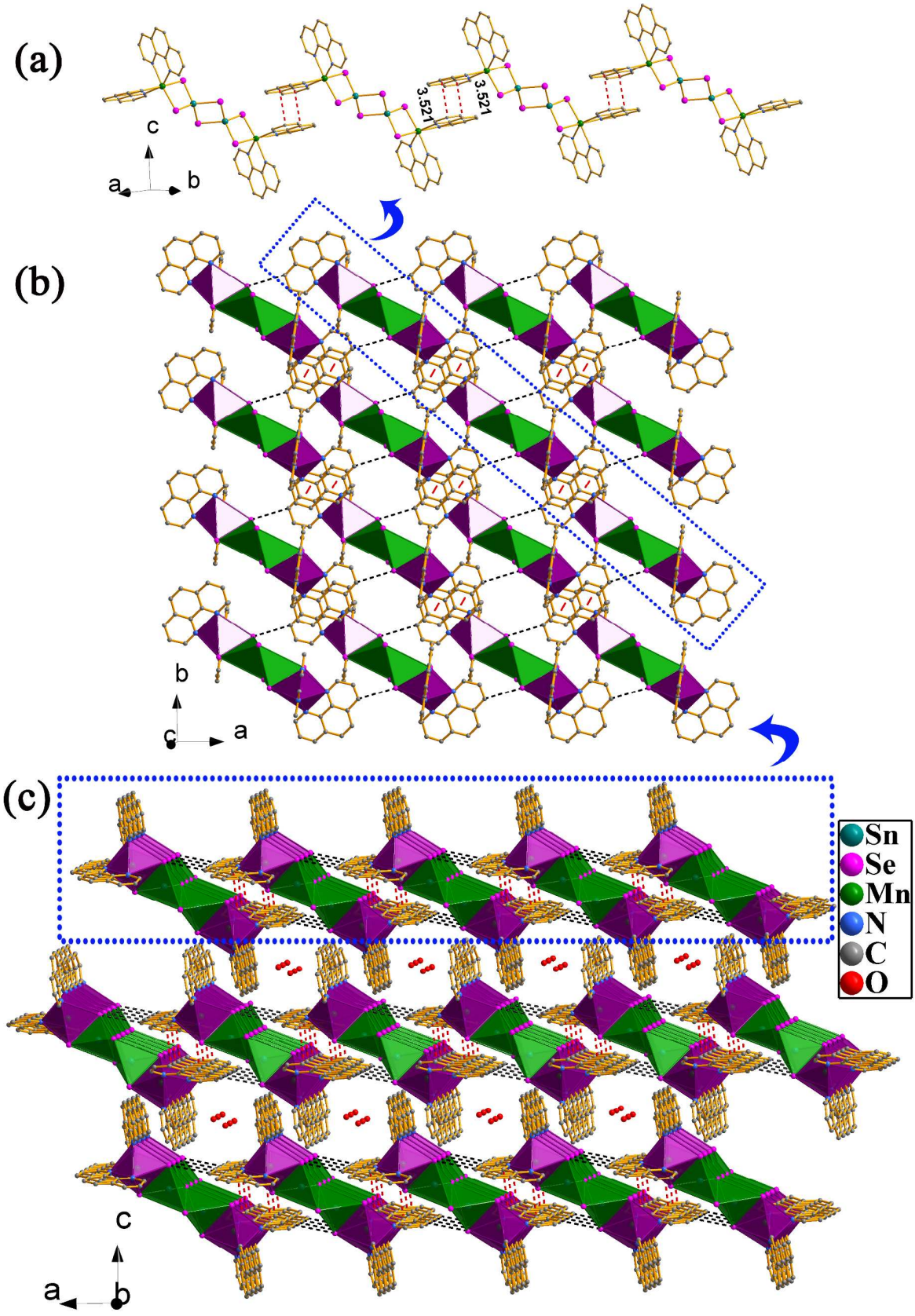


**Figure S5.** (a) View of a chain structure of **2a** assembled by the face-to-face $\pi\cdots\pi$ stacking interactions (red dashed lines). (b) Polyhedral representation of a 2-D extended layer structure

of **2a** showing hydrogen bonds (black dashed lines) and $\pi\cdots\pi$ stacking interactions. (3) 3-D packing diagram of **2a**. Purple octahedron: ($MnSe_2N_4$); green tetrahedron: ($SnSe_4$).

**Table S3.** Selected Hydrogen Bonds Data for **2a**.

| D–H···A | D–H (Å) | H···A (Å) | D···A (Å) | ∠(DHA) (°) |
|---|---|---|---|---|
| C13–H10C···Se1[a] | 0.93 | 2.95 | 3.675(4) | 136 |

Symmetry code: a 1+x, y, z.

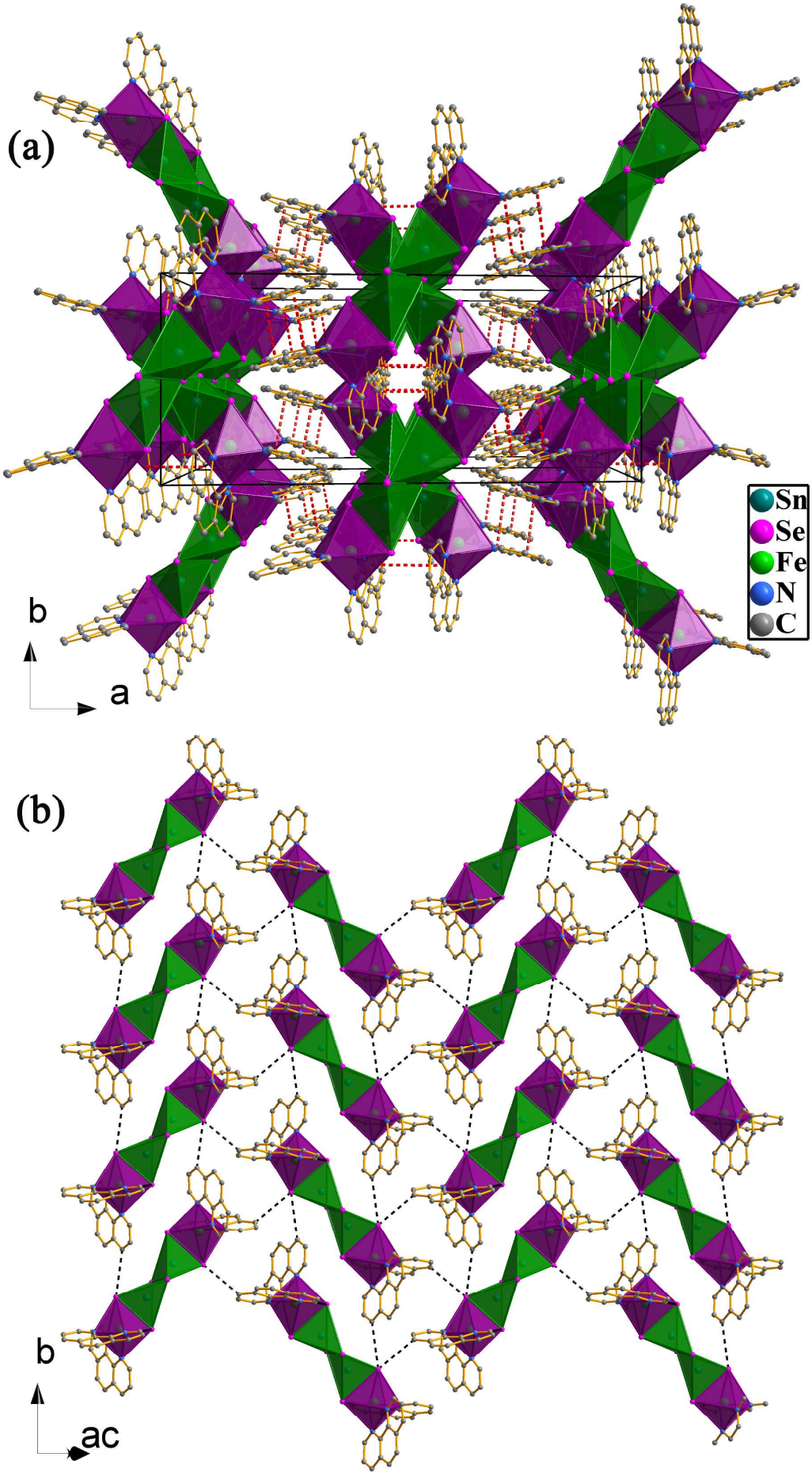
(a)
Sn
Se
Fe
N
C
b
a
(b)
b
ac

**Figure S6.** (a) Polyhedral view of the 3-D supramolecular framework of **2b** along the *c* axis assembled by the face-to-face $\pi\cdots\pi$ stacking interactions (red dashed lines). (b) Polyhedral view of a layer structure of **2b** assembled by the intermolecular C–H···Se hydrogen bonds (black dashed lines). Purple octahedron: ($MnSe_2N_4$); green tetrahedron: ($SnSe_4$).

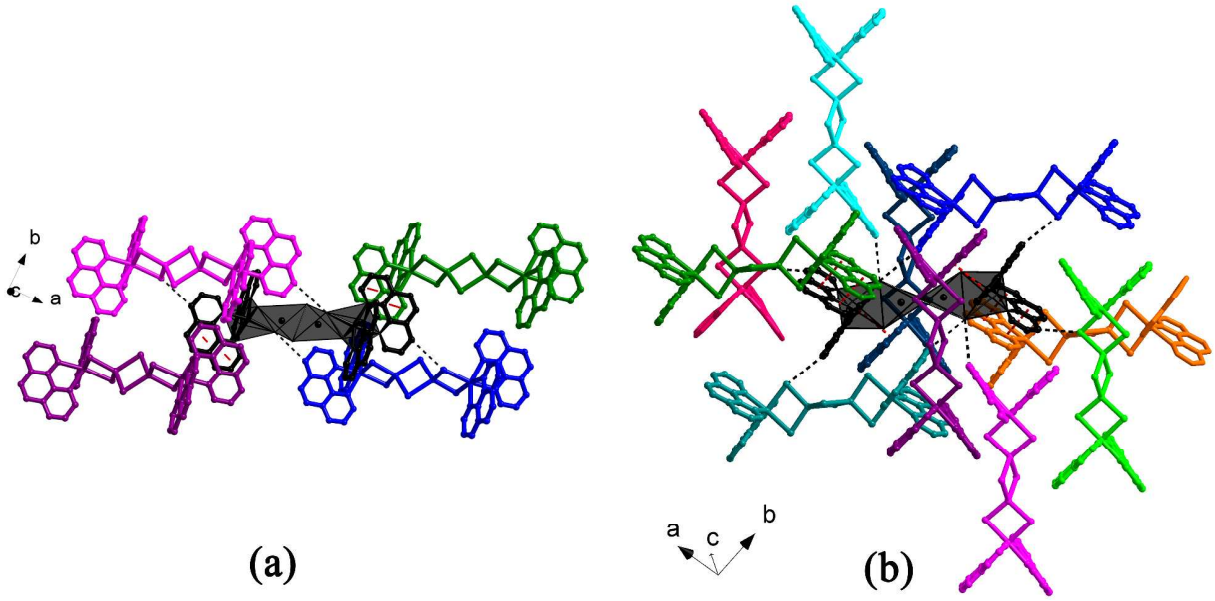


**Figure S7.** View of the surroundings of a neutral {[TM(phen)$_2$]$_2$($\mu_2$-$Sn_2Se_6$)} molecule (where the ($MnSe_2N_4$) and ($SnSe_4$) units are shown as black polyhedra) in **2a** (TM = Mn, (a)) and **2b** (TM = Fe, (b)), showing C–H···Se hydrogen bonds and face-to-face $\pi\cdots\pi$ stacking interactions.

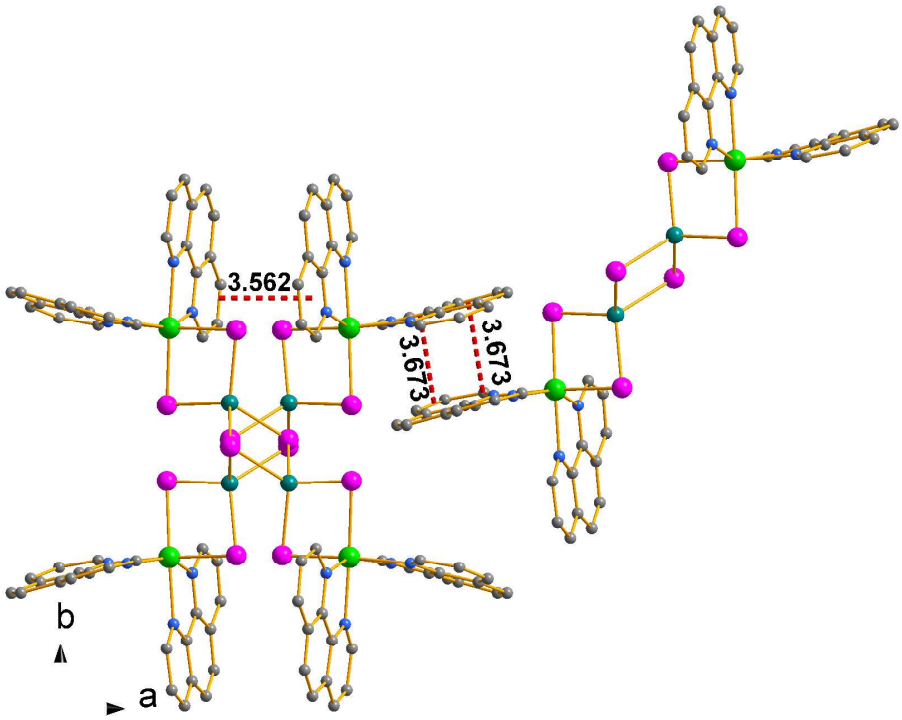


**Figure S8.** View of the face-to-face $\pi\cdots\pi$ stacking interactions in **2b** (red dashed lines).

**Table S4.** Selected Hydrogen Bonds Data for **2b**.

| D–H···A | D–H (Å) | H···A (Å) | D···A (Å) | ∠(DHA) (°) |
|---|---|---|---|---|
| C13–H13A···Se2[a] | 0.93 | 2.93 | 3.666(3) | 137 |
| C23–H23A···Se2[b] | 0.93 | 2.89 | 3.759(3) | 157 |

Symmetry codes: a 3/2-x,-1/2+y,3/2-z; b x,-1+y,z.

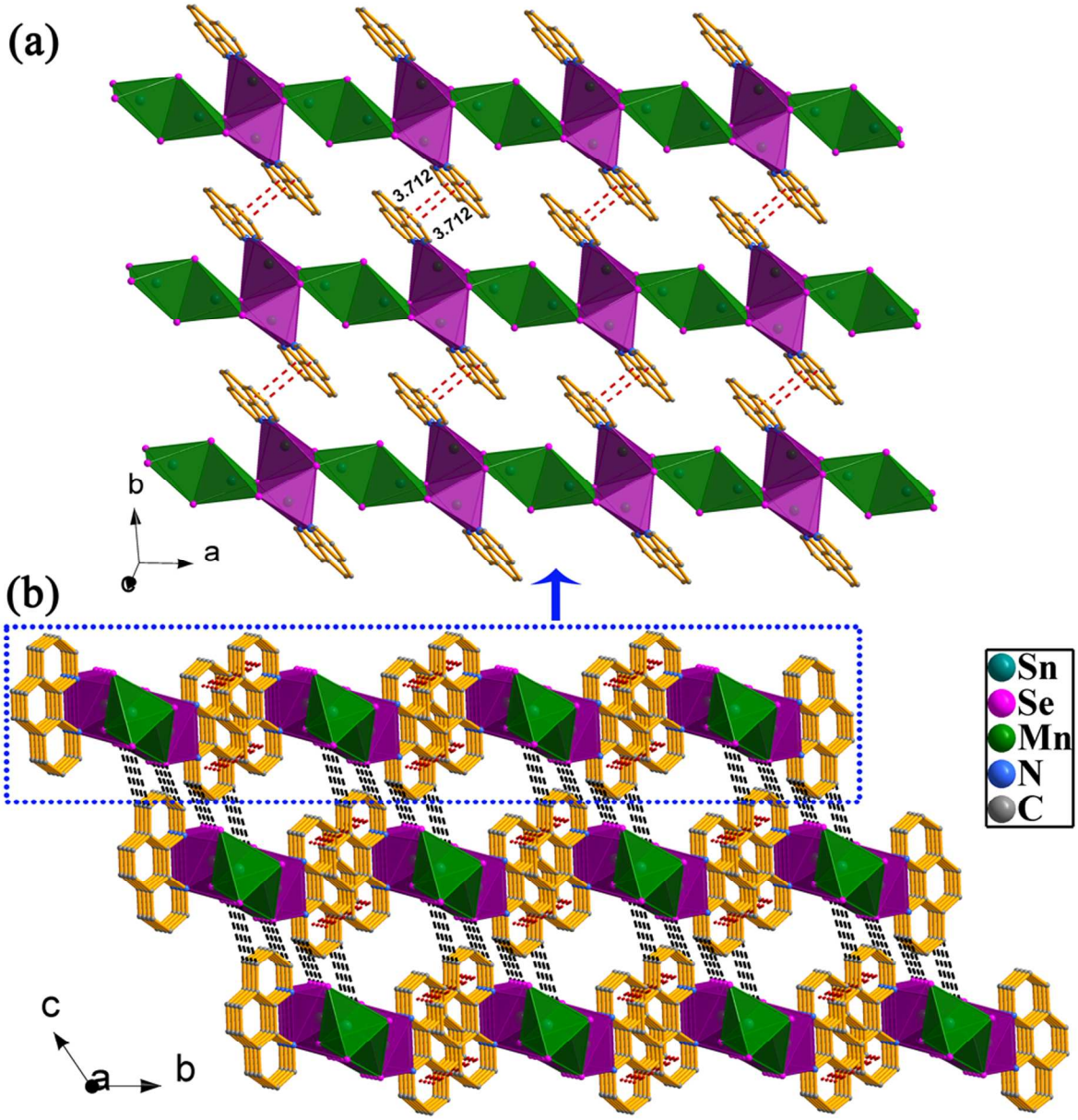


**Figure S9.** (a) Polyhedral representation of a 2-D extended layer structure of **3** showing $\pi\cdots\pi$ stacking interactions (red dashed lines). (b) Polyhedral view of the 3-D supramolecular framework of **3** along the *a* axis showing hydrogen bonds (black dashed lines) and $\pi\cdots\pi$ stacking interactions. Purple octahedron: ($MnSe_3N_2$); green tetrahedron: ($SnSe_4$). Hydrogen atoms are omitted for clarity.

**Table S5.** Selected Hydrogen Bonds Data for **3**.

| D–H···A | D–H (Å) | H···A (Å) | D···A (Å) | ∠(DHA) (°) |
|---|---|---|---|---|
| C3–H3A···Se2[a] | 0.93 | 2.92 | 3.691(4) | 141 |

| | | | | |
|---|---|---|---|---|
| C1–H1A···Se3[b] | 0.93 | 3.20 | 3.693(4) | 115 |

Symmetry code: a 1+x, y, 1+z; b 1-x, 1-y, 2-z.

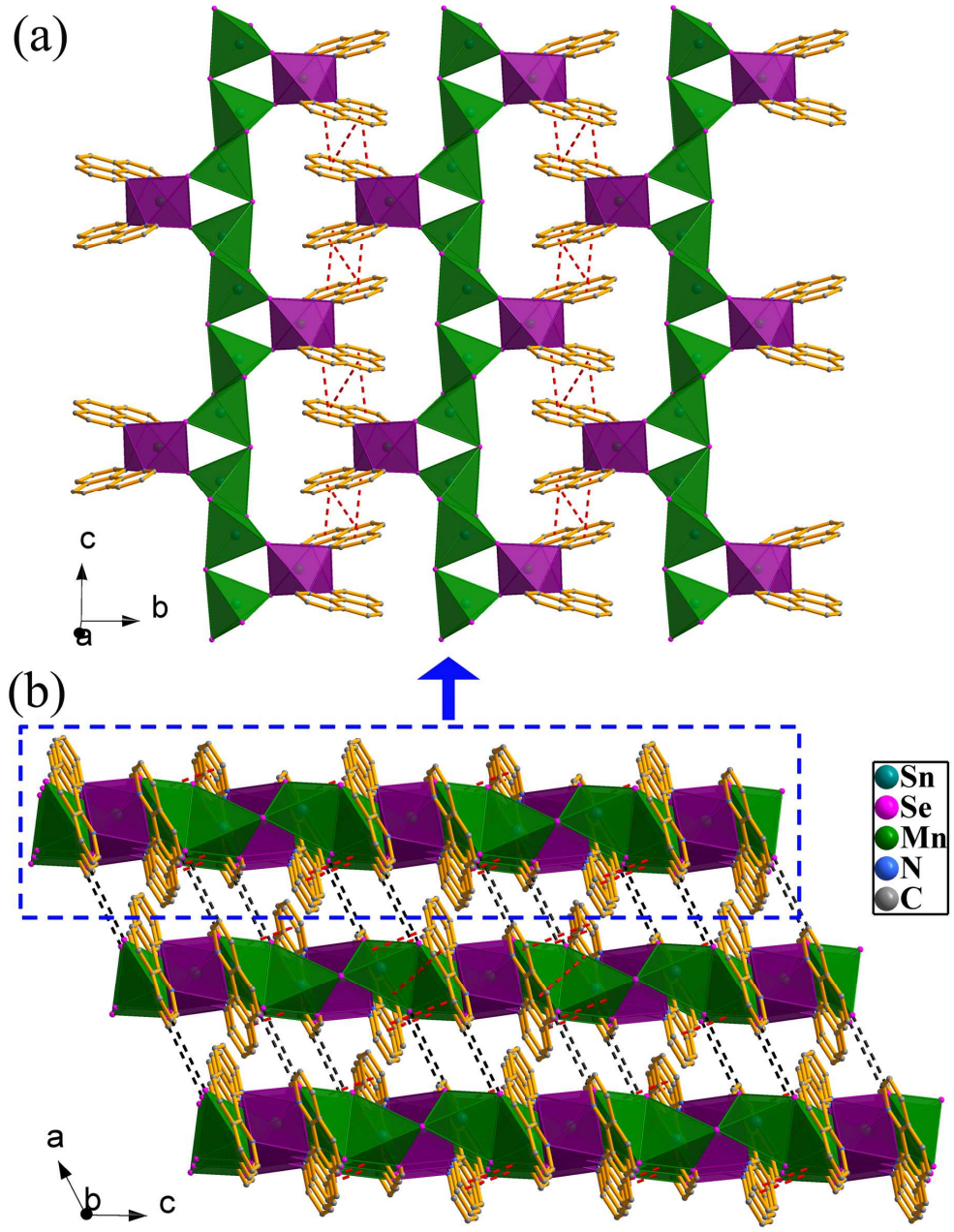


**Figure S10.** (a) Polyhedral representation of a 2-D extended layer structure of **4** showing $\pi\cdots\pi$ stacking interactions (red dashed lines). (b) Polyhedral view of the 3-D supramolecular framework of **4** along the *b* axis showing hydrogen bonds (black dashed lines) and $\pi\cdots\pi$ stacking interactions. Purple octahedron: ($MnSe_2N_4$); green tetrahedron: ($SnSe_4$). Hydrogen atoms are omitted for clarity.

**Table S6.** Selected Hydrogen Bonds Data for **4**.

| D–H···A | D–H (Å) | H···A (Å) | D···A (Å) | ∠(DHA) (°) |
|---|---|---|---|---|
| C19–H19A···Se3[a] | 0.93 | 3.03 | 3.779(4) | 139 |

Symmetry code: a 3/2-x, 1/2+y, 3/2-z.

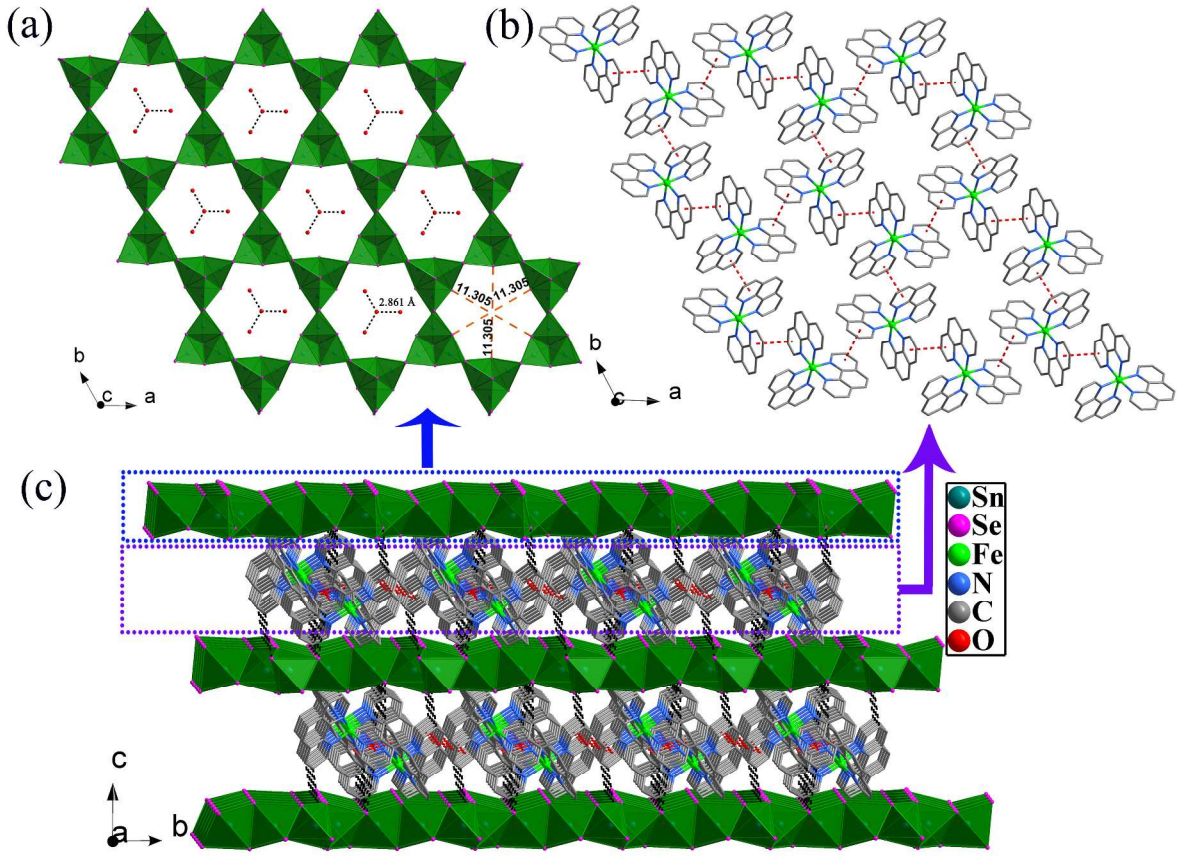


**Figure S11.** (a) Polyhedral representation of a $^{2}_{\infty}(Sn_3Se_7^{2-})$ layer structure of **5** with lattice water molecules residing in the honeycomb-like hole. (b) View of the 2-D extended layer structure of the $[Fe(phen)_3]^{2+}$ complex cations assembled by face-to face $\pi\cdots\pi$ stacking interactions (red dashed lines). (c) Polyhedral view of the 3-D supramolecular framework of **5** along the *a* axis. Green polyhedron: ($SnSe_5$). Hydrogen atoms are omitted for clarity.

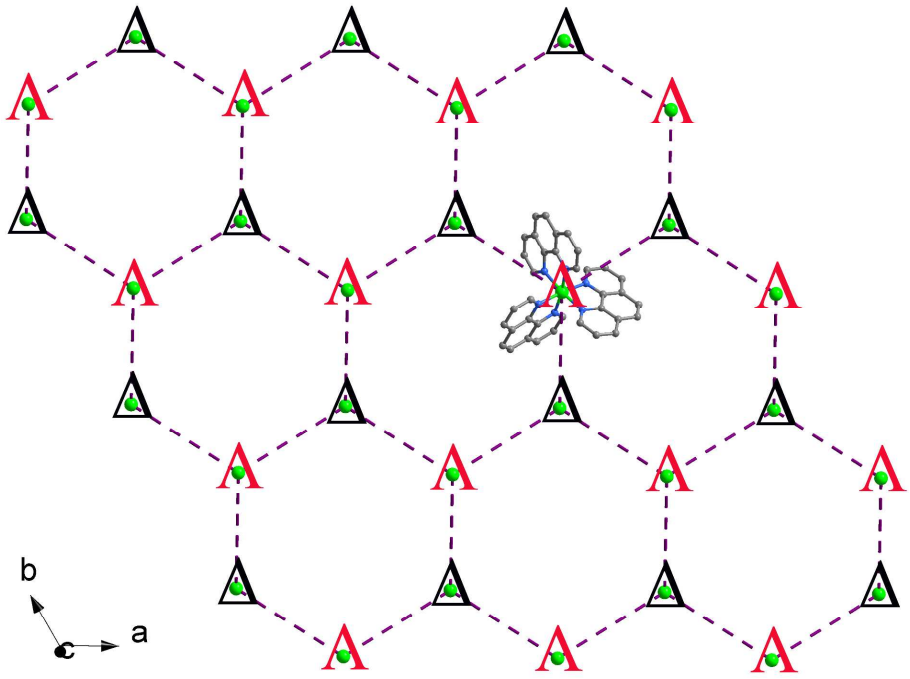


**Figure S12.** Topological view of the 2-D supramolecular $[Fe(phen)_3]_n^{2n+}$ layer of **5** with the $[Fe(phen)_3]^{2+}$ complex cation as a 3-connected node, and the configuration of the Fe complexes (Λ or Δ) labeled on the nodes.

**Table S7.** Selected Hydrogen Bonds Data for **5**.

| D–H···A | D–H (Å) | H···A (Å) | D···A (Å) | ∠(DHA) (°) |
|---|---|---|---|---|
| C9–H9A···Se1 | 0.93 | 2.97 | 3.716(4) | 138 |

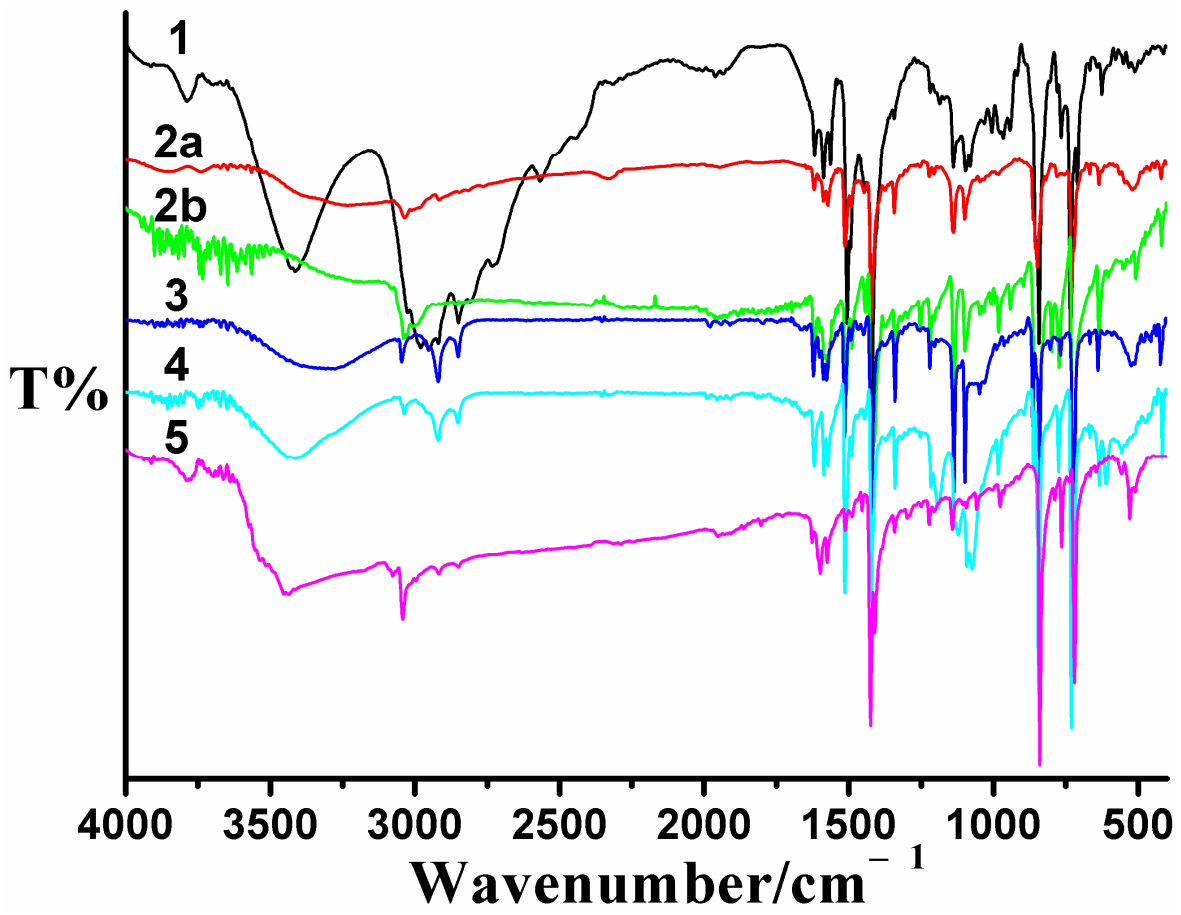


**Figure S13.** IR spectra of **1**–**5**.

In the IR spectra of **1**–**5** (Figure S13), the relatively weak bands in the region of 3081–3034 $cm^{-1}$ are attributed to the C–H vibrations of the aromatic ring hydrogen atoms, ν(=C–H). The bands of ring vibrations of the phen ligand (ν(C=C) and ν(C=N)) are observed at 1631–1415 $cm^{-1}$. Region 776–720 $cm^{-1}$ is attributed to δ(C–H), due to out of plane motion of hydrogen atoms of heterocyclic rings. For **1**, the IR bands at 2728 and 2564 $cm^{-1}$ correspond to the $–CH_3$ stretching and $–NH_3^+$ twisting vibrations, respectively. The occurrence of these resonance signals confirms the presence of mono-protonated methylamine molecules in **1**. The broad bands in the range of 3446–3315 $cm^{-1}$ for **1** and **2b**–**4** are assigned to the stretching of trace water since the measurements were conducted in air, while the broad brand for **2a** and **5** is simultaneously ascribed to the trace water in air and its lattice water molecules.

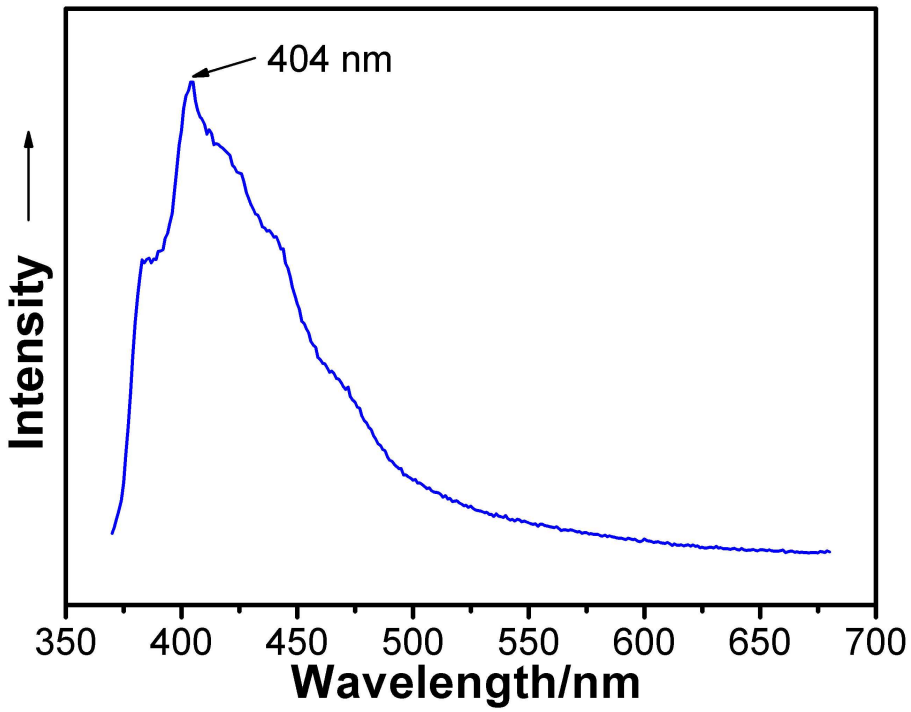


**Figure S14.** Solid-state photoluminescence spectrum of pure phen ligand measured at room temperature.

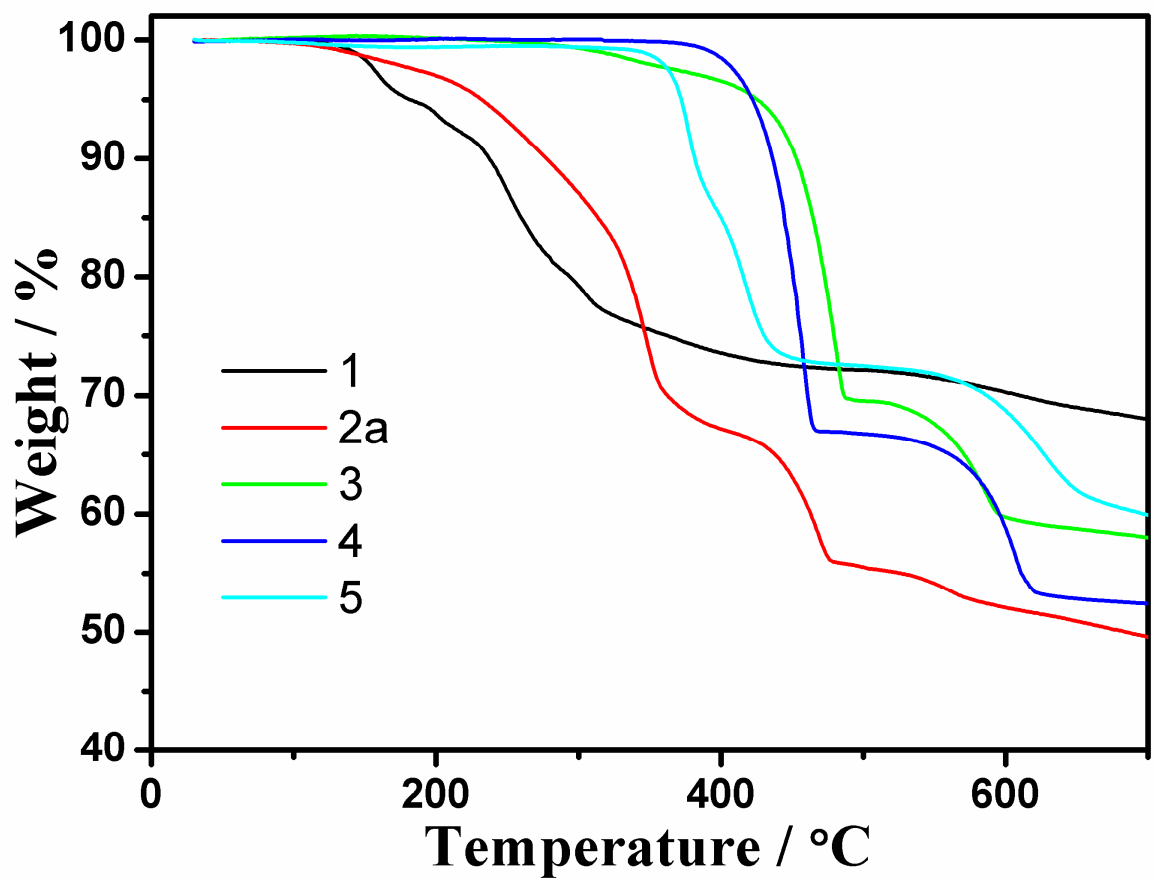


**Figure S15.** TGA curves of **1**, **2a** and **3**–**5**.

The thermal stabilities of **1**, **2a**, and **3**–**5** were examined by thermogravimetric analyses (TGA) in a $N_2$ atmosphere from 30 to 700 °C with the TGA curves shown in Figure S15. The TGA curve of **1** shows that compound **1** is stable up to 114 °C. A total weight loss of 8.4% in the temperature range 114–223 °C is attributed to the removal of four methylamine (calcd: 6.5%) and two $H_2S$ (3.6%) molecules per formula and the weight loss occurred in the temperature range 223–700 °C is consistent with the removal of the phen molecules. TGA for **2a** revealed a small weight loss of 1.9% between 84 and 169 °C, which corresponds to the removal of one lattice water molecule per formula (calcd: 1.1%). Further two-step weight losses from 169 to 508 °C with a significant weight loss of 44.6% is in agreement with the release of four phen molecules per formula (calcd: 45.7%). From the shape of the curve of **3**, it can be seen that the phen ligands are lost in one main step, and the observed weight loss of 30.4% in the temperature range of 262–501 °C agrees well with the calculated value of 30.5%. Compound **4** is more stable than **1**, **2a**, and **3**, and displays a clean one step loss with the

decomposition temperature at 353 °C. The corresponding weight loss of 33.2% to 505 °C is comparable with the complete loss of the phen molecules (calcd: 34.4%). For **5**, a small weight change of 0.7% in the temperature range of 59–203 °C is attributed to the removal of the lattice water molecules (calcd: 1.5%), and the following weight loss of 39.7% before 683 °C is comparable with the complete loss of the phen molecules (calcd: 35.4%).